

Recombination Lines and Free-Free Continua Formed in Asymptotic Ionized Winds: Analytic solution for the radiative transfer

Richard Ignace*

Department of Physics & Astronomy, East Tennessee State University, Box 70652, Johnson City, TN 37614, USA

The dates of receipt and acceptance should be inserted later

Key words radiative transfer – stars: emission line, Be – stars: winds, outflows – stars: Wolf-Rayet – circumstellar matter

In dense hot star winds, the infrared and radio continua are dominated by free-free opacity and recombination emission line spectra. In the case of a spherically symmetric outflow that is isothermal and expanding at constant radial speed, the radiative transfer for the continuum emission from a dense wind is analytic. Even the emission profile shape for a recombination line can be derived. Key to these derivations is that the opacity scales with only the square of the density. These results are well-known. Here an extension of the derivation is developed that also allows for line blends and the inclusion of an additional power-law dependence beyond just the density dependence. The additional power-law is promoted as a representation of a radius dependent clumping factor. It is shown that differences in the line widths and equivalent widths of the emission lines depend on the steepness of the clumping power-law. Assuming relative level populations in LTE in the upper levels of He II, an illustrative application of the model to *Spitzer*/IRS spectral data of the carbon-rich star WR 90 is given.

© 0000 WILEY-VCH Verlag GmbH & Co. KGaA, Weinheim

1 Introduction

The winds of massive stars are exceedingly dense, especially in evolved stars such as OB supergiants, Luminous Blue Variables (LBVs), and Wolf-Rayet (WR) stars (e.g., Cassinelli 1979; Lamers & Cassinelli 1999; Kudritzki & Puls 2000). The winds are dense and highly ionized, to the point where free-free opacity can become optically thick in the wind not only at radio wavelengths but also in the infrared (IR). Consequently, the IR band offers opportunities to study the wind density distribution through continuum and line emission. Wright & Barlow (1975) showed that at radio wavelengths the specific flux of emission for a spherical, constant expansion, isothermal, and optically thick wind will produce a continuum power-law having a slope of $f_\nu \propto \nu^{0.6}$, where f_ν is the specific flux (e.g., in Janskys). Knowing the distance to the star, the specific luminosity is derivable and can be related to the wind mass-loss rate \dot{M} . Observations of appropriate sources at radio frequencies have been important for deriving \dot{M} values (e.g., Abbott et al. 1980; Leitherer, Chapman, & Koribalski 1995).

Understanding mass loss during the various evolutionary stages of massive stars is of critical importance, as for example in understanding observed ratios of blue and red supergiant stars or the relative numbers of WR subtypes, the nitrogen, carbon, and oxygen rich WR stars (Maeder & Meynet 2000; Meynet & Maeder 2003). Mass-loss rates

are also important for interpreting the afterglows of gamma-ray bursts, of which some are associated with supernova explosions (Woosley & Bloom 2006).

Abbott, Biegging, & Churchwell (1981) showed that radio emission used to infer mass-loss rates can also depend on “clumping” if stellar winds are not laminar or “smooth”. The reason is that the free-free opacity scales with the square of the wind density. As a result, more or less clumping biases the mass-loss rate determinations if clumping corrections are not taken into account, with ramifications for our understanding of massive star evolution. And not only will clumping affect mass-loss rates, it can even have feedback for the line-driving efficiency of the winds in some cases (Brown et al. 2004; Oskinova, Hamann, & Feldmeier 2007).

It has become abundantly clear that stellar winds are indeed clumped, and that the clumping is not negligible in relation to interpreting \dot{M} values. Already, researchers had good reason to expect clumping to be important, since the hot star winds are understood to be line-driven (Castor, Abbott, & Klein 1975; Friend & Abbott 1986; Pauldrach, Puls, & Kudritzki 1986), a mechanism that is subject to instability leading to the formation of wind structure (Lucy & Solomon 1970; Owocki, Castor, & Rybicki 1988; Feldmeier, Puls, & Pauldrach 1997). Evidence for clumping in WR star winds and now even O star winds has been mounting for many years. In the case of WR stars, a convincing argument was made by Hillier (1991) on the basis of the emission of recombination line cores

* Email: ignace@etsu.edu

in relation to the strength of the electron scattering wings of the lines. The former is a density square process and subject to influence by clumping, but the latter is linear in density. Smooth wind models were found inadequate in matching the line profile shapes, but the inclusion of clumping allowed for superior matches between models and data.

Information about the clumping in the less dense winds of O stars has come only more recently (Bouret et al. 2003; Evans et al. 2004; Bouret, Lanz, & Hillier 2005). Indeed, quite startling results have been reported by Fullerton, Massa, & Prinja (2006) who suggest that on the basis of FUV doublet lines of P v that early O star mass-loss rates might need downward revisions by factors of 10 to perhaps 100. This result along with the general recognition of the prevalence of clumping in massive star winds led to an entire meeting devoted to the topic (Hamann, Feldmeier, & Oskinova 2007).

Many researchers have shifted attention from the question of whether the wind clumping exists to its origin and evolution (i.e., how clumping initiates, how it evolves through the wind, and how its nature changes with stellar evolutionary phase). A better understanding of clumping requires fresh considerations of what diagnostics may be used to constrain clump properties, such as size and mass distribution and dynamics. For example, Nugis, Crowther, & Willis (1998) considered how a gradient in the clumping factor with radius in the wind modifies continuum slopes for the wind emission. The main point of their study is that a constant clumping factor affects the amount of emission, but it does *not* change the observed power-law slope of the continuum. Only a clumping factor that is radius dependent will influence the slope.

Using the results of hydrodynamic simulations, Runacres & Owocki (2002, 2005) have considered how a structured flow evolves in radius for 1-dimensional wind models. Necessarily, such models predict clumping in the form of spherical shells. This has long known not to be an accurate description of hot star winds, for example owing to the relatively low variability observed in the X-ray emissions from massive stars (Cassinelli & Swank 1983; Berghöfer 1997). Indeed, there have been attempts to model the low X-ray variability in terms of statistically spherical but 3-dimensionally structured wind flow (Oskinova et al. 2001). Although impressive progress has been made in extending the 1-dimensional numerical simulations to an axisymmetric geometry (Dessart & Owocki 2002, 2003, 2005), the problem of fully 3-dimensional and time-dependent radiative hydrodynamic models remains a challenge.

With so much emphasis being given to measuring wind clumping factors and understanding structured wind flow, useful insight and tools can be gained from considering some simplified cases. As was noted, Wright & Barlow

(1975) were able to derive a power-law continuum slope of index $f_\nu \propto \nu^{0.6}$ at radio wavelengths for a spherical, isothermal, and inverse square law density. Still assuming a smooth wind flow, Cassinelli & Hartmann (1977) extended the approach to allow for power-law density and temperature distributions. They derived analytic expressions for the continuum slope. And indeed, IR spectra of WR winds are known to be steeper than the canonical $\nu^{0.6}$ rule (e.g., Morris et al. 1993), and so approaches like that of Cassinelli & Hartmann are relevant.

Emission line profile shapes have also been considered. Hillier, Jones, & Hyland (1983) derived an analytic solution for the radiative transfer of the line and continuum emission for density-squared opacities. For the continuum part, the standard Wright & Barlow (1975) solution is recovered in terms of the dependence on the wind parameters and the power-law scaling in frequency. The inclusion of continuous opacity and line optical depth in the Sobolev approximation yields a line profile shape that is centrally peaked and gently rounded in appearance (see Ignace, Quigley, & Cassinelli 2003).

Here the Hillier et al. (1983) solution is extended in two significant ways. First, their derivation prescribes a r^{-2} dependence for the wind density, but an additional power-law factor in radius can also be included in the opacity. Such a power law may represent the effects of a radius-dependent clumping factor. Second, it turns out that the radiative transfer can allow for an *arbitrary* number of line blends, which is important for IR spectra dominated by emission lines. The result of the new formulation is an analytic solution to a fairly complex scenario of line blends and power-law opacity but in the restrictive limit of spherical symmetry and constant expansion. Although direct applications may be limited, the solution provides complex cases against which sophisticated radiative transfer routines can be benchmarked.

The following section describes the approach to the analytic solution that extends the results of Hillier et al. (1983), following the notation of Ignace et al. (2003). Section 3 provides an illustrative application to high resolution spectra of the carbon-rich WC star, WR 90. A summary of results is given in section 4.

2 Radiative Transfer Solution

2.1 The Physical Ingredients

The scenario being addressed assumes spherical symmetry for a wind expanding at constant radial speed. For a fixed mass-loss rate, this means that the density is an inverse square law, hence

$$\rho = \frac{\dot{M}}{4\pi v_\infty r^2}. \quad (1)$$

Only continuum and line processes that scale with the square of the density will be considered. This is a reasonable approximation for dense, ionized winds of hot stars where free-free continuum opacity and recombination line opacity are important. The wind will be assumed isothermal. For the line transfer, the Sobolev approximation will be adopted.

Keys to the continuum radiative transfer are the expressions for the continuum and line optical depths. For free-free opacity, the optical depth from the observer to a point in the wind is

$$\tau_{\nu, \text{ff}} = R_* K_{\text{ff}}(T, \nu) \int_z^\infty n_i n_e dz', \quad (2)$$

where R_* is the radius of the star, n_i is the ion number density, n_e is the electron number density, and T is the isothermal temperature. Coordinates normalized to the stellar radius are used, with (p, ϕ, z) for cylindrical coordinates and (x, θ, ϕ) for spherical coordinates. The factor K_{ff} is given by (Cox 2000):

$$K_{\text{ff}} = 3.692 \times 10^8 \left(1 - e^{-h\nu/kT}\right) Z_i^2 g_\nu T^{-1/2} \nu^{-3}, \quad (3)$$

where g_ν is the Gaunt factor and Z_i is the root mean square ion charge. For the Gaunt factor at IR wavelength, a power-law in frequency is adopted as given by Carciofi & Bjorkman (2006),

$$g_\nu = g_0 (\nu/\nu_0)^{-u}, \quad (4)$$

with $u \approx 0.23$ at a frequency ν_0 corresponding to $1 \mu\text{m}$. Note that the number density quantities relate to the mass density in terms of mean molecular weights per ion μ_i and per free electron μ_e , respectively. Hence $\mu_i m_H n_i = \mu_e m_H n_e = \rho$.

The next step is to consider the line transfer, for which the Sobolev approximation is used. Although the wind is in constant radial expansion, a line-of-sight gradient in the projected line-of-sight velocity occurs owing to the divergent expansion of the spherical wind. Since highly supersonic wind speeds are of interest, the Sobolev approximation remains valid except for the extreme line wings where spatially the velocity gradient vanishes along the sightline from the observer to the star center.

For constant radial expansion, the observed Doppler shift in velocity units along the z -axis is

$$v_z = -v_\infty \cos \theta = -v_\infty \mu, \quad (5)$$

where θ is the spherical polar angle from the z -axis as previously noted, and $\mu = \cos \theta$. The main value of the Sobolev approximation is the identification of emission at a fixed velocity shift in an observed line profile with a spatial locus of points in the flow (or “isovelocity zones”). In this case a fixed velocity shift transforms to a conical surface in the spherical wind.

Sobolev theory does more than simply identify isovelocity zones. It also offers a solution to the line transfer (e.g., Castor 1970; Rybicki & Hummer 1978; Hummer & Rybicki 1983, 1985). It is known that Sobolev theory for modeling line profiles under the assumption of a smooth hot star wind is inadequate for producing realistic fits to some spectral features, such as the “black troughs” of ultraviolet P Cygni lines (Prinja, Barlow, & Howarth 1990). The problem is that not only are hot star winds clumpy in density, but the radial profile of the wind velocity is non-monotonic (Lucy & Solomon 1970; Lucy 1982). As a practical matter of line profile synthesis, the radiative transfer has been addressed by some in the form of a modified Sobolev approach, such as the SEI method of Lamers, Cerruti-Sola, & Perinotto (1987) or the co-moving frame methods of Hillier & Miller (1998) or Gräfener, Koesterke, & Hamann (2002). The non-monotonic behavior is approximated as an average smooth wind with substantial “turbulent” broadening (e.g., Groenewegen & Lamers 1989).

Since the Sobolev approximation is related to velocity gradients, it may be inappropriate for wind clumps if gradients are absent throughout such structures. However, the situation may not be so grave for the Sobolev approximation. First, a good model for the 3-dimensional structure (density and velocity) is currently lacking, and so the absence of velocity gradients remains a question. Second, in the scenario of this paper, the flow is treated as being in constant expansion, and the velocity gradient reduces to a geometrical one (see below) owing to spherical divergence, and clumps can certainly be expected to participate in the overall bulk radial expansion. Finally, the Sobolev approximation should remain valid for clumps that are small compared to the Sobolev length (i.e., $L \sim v_{\text{br}}/(dv_z/dr)$ for v_{br} the dominant local broadening process) and that are optically thin (in contrast to treatments of thick clumps as in Oskinova et al. 2007). Although limitations for the line transfer in the Sobolev approach are noted, Sobolev is employed to the restricted problem at hand to explore the influence of clumping on emission lines and continuum formation at long wavelengths.

The key parameter for describing the line transfer is the Sobolev optical depth τ_S for a line with opacity at point (p, ϕ, z) ; the optical depth is given by

$$\tau_S = \frac{\kappa_L \rho \lambda_0 R_*}{|dv_z/dz|}, \quad (6)$$

where κ_L is the frequency integrated line opacity with dimensions of area per mass times frequency, λ_0 is the central wavelength of the line transition, and the denominator is the line-of-sight velocity gradient evaluated at the isovelocity zone for fixed impact parameter p . The param-

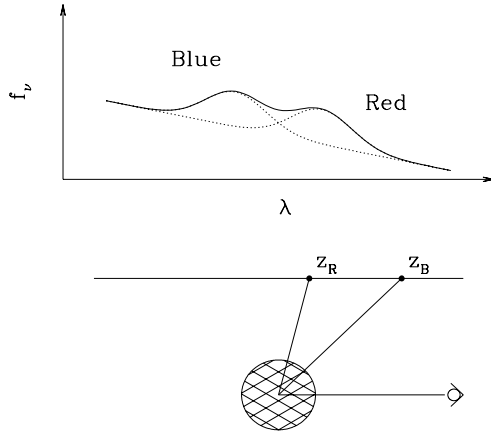


Fig. 1 Lower: A sightline that passes through the wind. The two points are intersections of the sightline with two different isovelocity cones shown here in cross-section. The geometry is for a line blend, such that at fixed λ , the transition with line center redward (“R”) of λ is the rearward point, and the one that is blueward (“B”) is nearer the observer. Above is a cartoon illustration of a line blend that might emerge from the wind, with solid for the total and dotted for the individual line contributions.

eter R_* appears because z is a normalized coordinate. In spherical symmetry the velocity gradient becomes

$$\frac{dv_z}{dz} = \frac{dv}{dx} \cos^2 \theta + \frac{v}{x} \sin^2 \theta, \quad (7)$$

where $x = r/R_*$. Equation (7) reduces to $(v_\infty/x)(1 - \mu^2)$ for a wind in constant expansion.

2.2 The Solution to the Radiative Transfer

2.2.1 Solution for General Line Source Functions

Before embarking on the steps of the derivation, more parameters must be introduced to describe the properties of the radiation. The continuum source function is represented by S_C , which for free-free processes is Planckian, hence $S_C = B_\nu(T)$. The line source function will be S_L .

The derivation largely follows the notation of Ignace et al. (2003) who elaborated on the steps originally described by Hillier et al. (1983). For $S_L = S_C = B_\nu(T)$, the total emergent intensity of continuum and line radiation is given by (eq. [A1] of Ignace et al.):

$$I_\nu = B_\nu \left[1 - e^{-(\tau_{\max} + \tau_S)} \right], \quad (8)$$

where τ_S is evaluated at the point (p, z) , and τ_{\max} is the maximum free-free optical depth along a sightline. The assumption of an isothermal wind is implicit in equation (8) so that B_ν may be factored out of the integral to obtain a solution to the transfer equation.

As in Ignace et al., it is convenient to express continuum and line optical depths in terms of scale parameters τ_C and τ_L that encompass the various physical properties of the wind and opacity that do not vary with spatial location (such as T, ν , etc). The Sobolev and optical depth can be expressed as:

$$\tau_S = \tau_L x^{-3} (1 - \mu^2) = \tau_L \sin \theta p^{-3}. \quad (9)$$

which uses the fact that $p = x \sin \theta$. The continuum free-free optical depth from the observer to any point z in the wind along a fixed sightline of impact parameter p derives from an integral along the path as given by

$$\tau_{\text{ff}} = \tau_C \int_z^\infty \frac{dz}{x^4 w^2(x)}. \quad (10)$$

Eliminating x again in favor of p and θ , the integral for the continuum optical depth has an analytic solution given by

$$\tau_{\text{ff}} = \frac{\tau_C}{2p^3} (\theta - \sin \theta \cos \theta) \quad (11)$$

where $\tan \theta = p/z$. The parameter τ_C is a scaling parameter for the free-free optical depth that incorporates the various wind and atomic constants involved along with the frequency dependence; in relation to equation (2), it is given by:

$$\tau_C = R_* K_{\text{ff}}(T, \nu) n_{i,0} n_{e,0}, \quad (12)$$

where $n_{i,0}$ and $n_{e,0}$ are the ion and electron number densities at the wind base R_* . The maximum optical depth τ_{\max} along a sightline that does not intercept the stellar photosphere is

$$\tau_{\max} = \frac{\pi \tau_C}{2p^3}. \quad (13)$$

When $\tau_{\text{ff}} \gg 1$, an IR/radio pseudo-photosphere forms that is much larger than the hydrostatic stellar photosphere. In this case there is a standard integral that allows for the integration of the emergent intensity with impact parameter to derive the total flux of line and continuum radiation (Hillier et al. 1983). The new considerations include line blends, an additional power-law dependence to the opacity, and line source functions that need not be Planckian. Although a closed form for the emergent intensity can be given for this new generalization, there is unfortunately no analytic solution for the total flux, except in the special case of LTE for the line source functions. (That case will be considered in subsequent sections.)

In deriving the emergent intensity, the first of the new considerations is to allow for a line blend. Suppose there is a wavelength where two separate lines contribute to the opacity. The two lines shall be referenced in terms of respective line center wavelengths as the “red” line (centered at λ_R) and the “blue” line (centered at λ_B) relative to the wavelength λ under consideration. As illustrated in Fig. 1, the velocity shift for the red line is necessarily at

an isovelocity zone that lies rearward of that for the blue line. Figure 1 shows a sightline as it might cross the two isovelocity zones (and no more!) for the two respective lines at wavelength λ . The following equation describes contributions from alternating emission and attenuations by the respective line and continuum opacities in the different segments of the figure as working from left to right:

$$\begin{aligned} I_\nu = & B_\nu (e^{-\tau_R} - e^{-\tau_{\max}}) e^{-\tau_{S,R}} e^{-\tau_{S,B}} \\ & + S_R (1 - e^{-\tau_{S,R}}) e^{-\tau_R} e^{-\tau_{S,B}} \\ & + B_\nu (e^{-\tau_B} - e^{-\tau_R}) e^{-\tau_{S,B}} \\ & + S_B (1 - e^{-\tau_{S,B}}) e^{-\tau_B} \\ & + B_\nu (1 - e^{-\tau_B}), \end{aligned} \quad (14)$$

There is an identifiable pattern that can be extended to allow for blends of an arbitrary number of lines. It is convenient to split the emergent intensity into two parts: the continuum contribution I_C arising from terms with the continuum source function and I_L involving contributions from all of the line source functions.

The emergent intensity from the free-free continuum emission is given by

$$\begin{aligned} I_C = & B_\nu \left[1 - \sum_{j=1}^{N+1} e^{-\tau_j} \exp \left(- \sum_{i=0}^{j-1} \tau_{S,i} \right) \right. \\ & \left. + \sum_{j=1}^N e^{-\tau_j} \exp \left(- \sum_{i=1}^j \tau_{S,i} \right) \right], \end{aligned} \quad (15)$$

where N is the total number of lines contributing to the blend at a fixed frequency in the spectrum. In this formulation τ_i is the free-free continuum optical depth from the observer to the i^{th} resonance point along a given ray through the wind. In this notation $\tau_{N+1} = \tau_{\max}$. Then $\tau_{S,i}$ is the Sobolev optical depth at the i^{th} resonance point, with $\tau_{S,0} \equiv 0$.

The contribution of the total line intensity is given by

$$I_L = \sum_{i=1}^N S_i (1 - e^{-\tau_{S,i}}) e^{-\tau_i} \exp \left(- \sum_{j=0}^{i-1} \tau_{S,j} \right). \quad (16)$$

Note that at this point, the only requirement on the solution for equations (15) and (16) is that the wind be isothermal; velocity structure, ionization gradients, or variable clumping factors are allowed in the set of continuum optical depths τ_j . The set of line optical depths $\tau_{S,i}$ are also quite general since they are locally evaluated only at crossings of the sightline with isovelocity zones. Indeed, it is not even necessary at this point to specify the velocity law or the geometry of the isovelocity zones; that information

is only required when evaluating the total flux of emission. Given that B_ν is constant, the above relations result only from a consideration of sequencing.

The total emergent intensity along the ray is simply $I_\nu = I_C + I_L$. In order to obtain the continuum spectral distribution and line profile shapes, additional simplifying assumptions of constant expansion and $S_{L,i} = B_\nu$ are introduced next as a particular realization of possible wind models.

2.2.2 The Solution for LTE Source Functions

It is well-known that the level populations of atomic species in stellar winds is highly NLTE (Auer & Mihalas 1972). However, the application being considered here is for IR/radio spectra involving H I or He II recombination lines and free-free continua. The continuum that is formed at large radius and thus roughly coincident with the line formation is LTE. The lines themselves are for transitions involving high n -level values whose populations should be governed largely by recombination and photoionization processes. These lines are formed at sufficiently large radius that in the case of the WR winds, the EUV radiation from the star is (a) highly diluted and (b) strongly absorbed by the dense wind. In this case the photoionization from the spatially local IR continuum that is Planckian (although not isotropic) will contribute to the populations of the upper levels. Indeed, Hillier et al. (1983) found that the relative upper level populations for some high n -levels of He II in EZ CMa were consistent with LTE.

Here LTE is invoked as a convenience to allow for an analytic solution to the line and continuum fluxes and quick exploration of the model parameters. There is a tremendous simplification for the emergent continuum and line intensities, because all but two terms cancel exactly. After simplifying expression (14) using $S_R = S_B = B_\nu$, the emergent intensity reduces to just

$$I_\nu = B_\nu \left[1 - e^{-(\tau_{\max} + \tau_{S,R} + \tau_{S,B})} \right], \quad (17)$$

$$= B_\nu \left[1 - e^{-\tau_T} \right]. \quad (18)$$

where τ_T is a sum of all three optical depths. As before, this can be extended for an arbitrary number of line blends, now with $\tau_T = \tau_{\max} + \sum_{i=1}^N \tau_{S,i}$. Each Sobolev optical depth must be evaluated for its respective isovelocity zone at a fixed frequency. This amounts to different velocity shifts for lines of different wavelength centers $\{\lambda_i\}$. These shifts can be written in normalized form as $w_i = v_{z,i}/v_\infty = -\mu_i$. It is the total flux of emission that is required to simulate observables, and the intensity is now of a form that can be solved analytically because both the line and continuum optical depths have the same radial dependence.

Another important extension to previous treatments is that an *additional* power-law dependence of the opacity can be included. The winds are known to be clumped, and so this new power-law dependence can be used to represent a radius dependence of the clumping. The clumping factor D_C is introduced as follows:

$$D_C = \frac{\langle \rho^2 \rangle}{\langle \rho \rangle^2} \propto x^{-m}. \quad (19)$$

As a result, the Sobolev optical depth becomes

$$\tau_S = \tau_L x^{-(3+m)} (1 - \mu^2)^{-1} \quad (20)$$

$$= \tau_L p^{-(3+m)} (\sin \theta)^{1+m}, \quad (21)$$

where τ_L is a scale factor for the optical depth. Equation (21) in terms of p and θ will prove useful in evaluating the total flux. The free-free optical depth becomes

$$\tau_{\max} = \tau_C \int_{-\infty}^{\infty} x^{-(4+m)} dz \quad (22)$$

$$= \tau_C p^{-(3+m)} \int_0^\pi (\sin \theta)^{2+m} d\theta \quad (23)$$

$$\equiv \tau_C p^{-(3+m)} \times \gamma(m). \quad (24)$$

where τ_C from equation (12) is now expressed as

$$\tau_C = \frac{K_{\text{ff}}(T, \nu) \dot{M}^2}{16\pi^2 R_*^3 v_\infty^2 \mu_e \mu_i m_H^2} \quad (25)$$

and γ is a constant that depends solely on the power-law index m via the integral factor of equation (23). In the case that $m = 0$, $\gamma = \pi/2$. Formally, the latter expression only applies for rays that do not intersect the star, hence only for $p > 1$.

As discussed by Wright & Barlow (1975), as long as the continuum optical depth is quite large, a pseudophotosphere is formed that is significantly larger in cross-section than the star itself. In this case ignoring rays with $p < 1$ represents a small error in the flux. Under these circumstances, the solution for the total flux of emission in the continuum and lines is analytic. Even with line blends and the additional power-law factor, the form of the integral is similar to that of Ignace et al. (2003). Here the steps for deriving f_ν are reviewed.

The flux is given by an integral of the intensity over all rays:

$$f_\nu = 2\pi \frac{R_*^2}{d^2} \int_\nu I_\nu(p) p dp, \quad (26)$$

where the integral accounts for only those spatial points in the wind that contribute to emission for some frequency in the spectrum ν . Unlike the single line case considered in Ignace et al., this frequency point may have contributions

from multiple line opacity sources. Using equation (18) with constant B_ν , the flux becomes

$$f_\nu = 2\pi B_\nu \frac{R_*^2}{d^2} \int_0^\infty \left(1 - e^{-\tau_T(p)}\right) p dp, \quad (27)$$

where d is the distance to the star, and from equations (21) and (24) the total optical depth is now

$$\tau_T(p) = p^{-(3+m)} \times \left[\tau_C \gamma(m) + \sum_i^N \tau_{L,i} (\sin \theta_i)^{1+m} \right]. \quad (28)$$

Again, the use of the form of the total optical depth above in the preceding integral relation for the flux assumes that the flux contribution for rays with $p < 1$ is relatively small. This is a good approximation at long wavelengths because the effective photosphere can indeed be much larger than R_* . The advantage of this treatment is that the integral is analytic.

To arrive at the solution, it is useful to introduce a change of variable with $U^{(3+m)} = \tau_C p^{-(3+m)}$ to convert the integral expression to the following form:

$$f_\nu \approx 2\pi B_\nu \frac{R_*^2}{d^2} \int_0^\infty \tau_C^{2/(3+m)} U^{-3} dU \times \left\{ 1 - \exp \left[U^{3+m} \left(\gamma - \tau_C^{-1} \sum_{i=0}^N \tau_{L,i} \sin^{m+1} \theta_i \right) \right] \right\}, \quad (29)$$

where the sum refers to any of the lines contributing to the opacity at the frequency of interest. For $N = 0$ there are no contributing line opacities, $\tau_{L,0} = 0$, and expressions reduces to an expression for the continuum emission alone.

The integral in that form of (29) has a solution given in Gradshteyn & Ryzhik (2000) found in section 3.478, #2, with the final result for the observed flux f_ν being

$$f_\nu = 2\pi B_\nu \frac{R_*^2}{d^2} \tau_C^{2/(3+m)} \left[\frac{3+m}{2} \Gamma \left(\frac{1+m}{3+m} \right) \right] \times \left\{ \gamma(m) + \sum_{i=0}^N \frac{\tau_{L,i}}{\tau_C} (1 - w_i^2)^{(m+1)/2} \right\}^{2/(3+m)}, \quad (30)$$

where Γ is the Gamma-function, and $\sin \theta = (1 - w_z^2)^{1/2}$. For reference, the solution equation (30) shall be referred to as the “Free-free + Recombination Emission line in Constant velocity” model, or the “FREC” model.

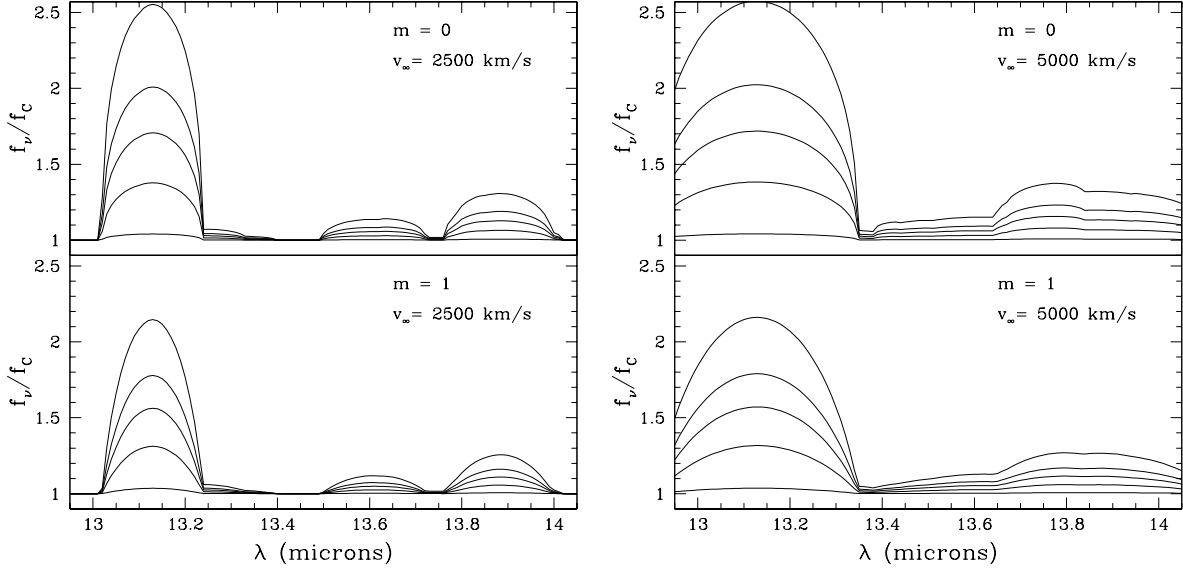


Fig. 2 Illustration of the analytic solution for a continuum dominated by free-free emission and He II recombination lines, such as occurs for WR stars. Spectra are shown as normalized to the continuum f_c . The two plots left and right are for two different wind terminal speeds as indicated. The upper and lower panels are for two different power law indices m : upper is for constant clumping factor and lower is for clumping that decreases inversely with radius. Note that the analytic results account fully for line blending. The different curves within each panel are for different line strengths.

In regions of the spectrum that are absent of lines, the FREC model provides the continuum flux. In the Rayleigh-Jeans limit, the continuum reduces exactly to a power-law form. Assuming $h\nu \ll kT$ and using the Gaunt factor of equation (4), the continuum distribution between lines becomes a function of just one free parameter m (i.e., for the value of u known):

$$f_\nu \propto \nu^{(2+2m)/(3+m)} g_\nu^{2/(3+m)} \propto \nu^{2(m+1-u)/(3+m)}. \quad (31)$$

Note that with u appropriate for the radio band, and $m = 0$, the 0.6 power-law slope of Wright & Barlow (1975) is recovered.

Returning to the lines, why does the line shape vary with m -value? Although both line and continuum opacities scale with the square of the density, the line optical depth has an additional dependence with angular escape through a velocity gradient. As a result, the line shape is not invariant with respect to the continuum formation as m is varied.

Examples of model spectra produced by the FREC solution are shown in Fig. 2. The models are continuum-normalized to focus on the line shape effects and the inclusion of blending. The left and right plots are for different wind speeds of 2500 and 5000 km s⁻¹. All panels show a segment of the 13–14 micron spectrum. All emission lines are of He II recombination; the strong line at 13.12 microns is He II 10 α . The upper panel is for $m = 0$, corresponding to a wind that has a constant clumping fac-

tor. The lower panel is for $m = 1$, indicating a clumping factor that decreases with radius.

To clarify better the line-shape dependence on the index m , it is useful to consider limiting cases of a single strong or weak line: a strong line occurs for $\tau_L \gg \tau_C$ and a weak one for $\tau_L \ll \tau_C$. A single strong line yields the profile shape given by

$$f_\nu \propto [1 - w^2]^{(1+m)/(3+m)}. \quad (32)$$

In the case of a weak line, the flux is of the form $f_\nu \propto 1 + \epsilon$, where ϵ has the functional dependence of

$$\epsilon \propto [1 - w^2]^{(1+m)/2}. \quad (33)$$

The profile shapes for thin and thick lines are not the same. Thick lines tend to be more “rounded” or “bubbled” as compared to thin ones. The half width at half maximum (HWHM) of a thick line is greater than for a thin one. In the case of a thick line, it is

$$\text{HWHM}_{\text{thick}} = v_\infty \sqrt{1 - \left(\frac{1}{2}\right)^{(3+m)/(1+m)}}, \quad (34)$$

whereas for a thin line, it is

$$\text{HWHM}_{\text{thin}} = v_\infty \sqrt{1 - \left(\frac{1}{2}\right)^{2/(1+m)}}. \quad (35)$$

For $m = 0$, $\text{HWHM}_{\text{thick}} = 0.94v_\infty$ and $\text{HWHM}_{\text{thin}} = 0.87v_\infty$. The difference in half-width from the full terminal speed is small, but it becomes greater for increasing values of m . With $m = 1$, the half-width values become $0.87v_\infty$ versus $0.71v_\infty$. For fast winds of WR stars

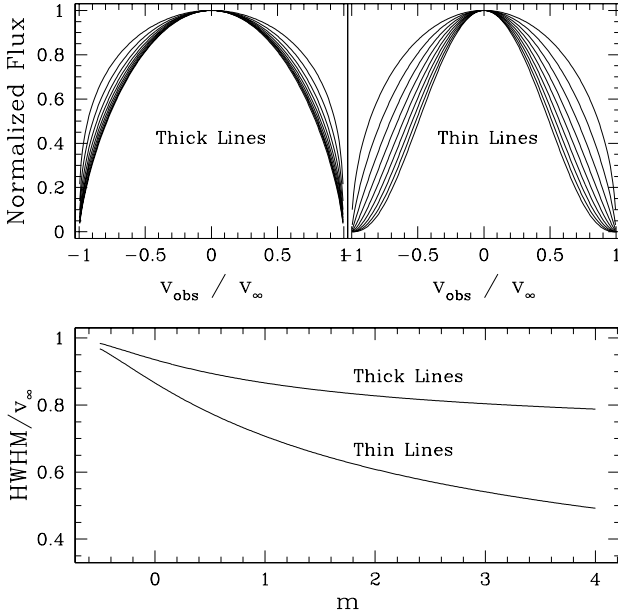


Fig. 3 Comparisons between thick and thin emission lines from the FREC model. The two top panels display line profiles for thick (left) and thin (right) lines. These are continuum subtracted and then normalized to their peak values and plotted against normalized velocity shift. Each curve is for a different m value, from $m = -0.5$ to 4 in intervals of 0.5. At bottom is a plot of the HWHM of thick and thin lines against m . The line widths are normalized to the wind terminal speed.

at around 2000 km s^{-1} , the difference amounts to over 300 km s^{-1} , which is potentially measurable. Figure 3 compares, as a function of m value, thick versus thin line profile shapes (top two panels) with a corresponding plot (bottom panel) of the HWHM values relative to the wind terminal speed.

It is also useful to consider trends in the line equivalent width (EW). The line equivalent width for the FREC model with a single line is given by:

$$EW = \frac{\lambda_0 v_\infty}{c} \times \int_{-1}^{+1} \left[1 + \frac{\tau_L}{\gamma(m) \tau_C} (1 - w^2)^{\frac{m+1}{2}} \right]^{\frac{2}{3+m}} dw, \quad (36)$$

where $w = v_{\text{obs}}/v_\infty$ is the normalized velocity shift across the line. Figure 4 shows curves for the EW normalized to $\lambda_0 v_\infty/c$ and plotted as a function of the relative line strength $\tau_L/\gamma(m) \tau_C$. The different curves are for different values of m at increments of 0.25. Curves are closely clustered with shallow slopes for larger values of m representing steeper declines in the clumping factor with radius in the wind.

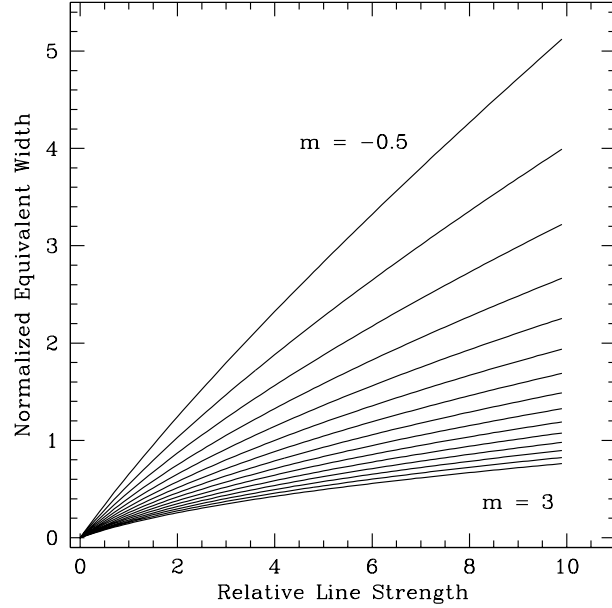


Fig. 4 Normalized line equivalent widths (EW) are plotted against the relative line strength (see text). Each curve is for a different power-law index m , ranging from $m = -0.5$ up to $m = 3$ in increments of 0.25. The EW is seen to grow in line strength as expected, but the rapidity of growth is much less for clumping factors that are more steeply decreasing with radius.

The overall result is that increasing values of m steepen the decline in clumping with radius, narrow the line width, increase the relative line strength (because γ decreases with m), and decrease the line EW . Equations (21) and (24) show how the line and continuum optical depths change with m , and the rate of decline for these is not the same along a fixed sightline. The line becomes thinner more rapidly at a given resonance point as compared to the total line-of-sight free-free optical depth.

3 Application to WR 90

With the solution to the radiative transfer through the wind at hand, it is useful to consider an illustrative model. The continuum slope is set by equation (31). To construct a full emission line spectrum, a tabulation of line optical depth scales $\{\tau_{L,i}\}$ are required as input to the model. The IR spectra of WR stars are characteristically He II emission line spectra, and at wavelengths longer than about 10 microns (relevant to the *Spitzer/IRS*), the line transitions involve somewhat high n -values, levels above $n = 9$.

With the LTE assumption, the Sobolev optical depth scale factors vary with the line transition as follows:

$$\tau_L \propto gf \lambda \left(\frac{n_i}{g_i} - \frac{n_j}{g_j} \right), \quad (37)$$

where f is the oscillator strength, g values are statistical weights for respective levels, and n is a scaled number density (i.e., no dependence on radius). Assuming the Rayleigh-Jeans limit as a simple case, the final result of this is that

$$\tau_L \propto gf \frac{n_j}{g_j} \propto \lambda^2 A_{ji} n_j. \quad (38)$$

It is now easy to compare the line optical scale factors for any two lines τ_L and τ'_L involving different upper levels j and j' . Given in ratio, the optical depth scales are related as follows,

$$\frac{\tau'_L}{\tau_L} = \left(\frac{\lambda'}{\lambda} \right)^2 \left(\frac{A'}{A} \right) \left(\frac{g'}{g} \right). \quad (39)$$

A FREC spectral model depends on just three items: (1) m that sets the continuum slope, (2) τ_0 a fiducial line optical depth for some line from which all other lines scale, and (3) a list of He II line data. An example application in Fig. 5 shows a FREC model overplotted with *Spitzer* IRS/SH data of the WC star, WR 90. Data are shown as solid, and the model is the dotted curve. Transitions for He II up to $n = 30$ are included. The observed spectrum includes lines of other atomic species besides just recombination lines of He II, notably the booming line of [Ne III] at 15.55 microns, but also lines from ionized carbon. The model makes no attempt to include any lines other than He II recombination lines. The dotted curve is the simple two-parameter spectral model as “eyeballed” for a good fit. The model does adopt the wind terminal speed of WR 90 from Ignace et al. (2007) and has been gaussian convolved to match the resolution of the IRS in SH mode.

A value of $m = 0.9$ reasonably reproduces the observed slope. After fixing the continuum slope, the optical depth scale was varied until approximate matches to the observed emission in He II 10α at $13.12 \mu\text{m}$ and 11α at $17.26 \mu\text{m}$ were achieved. The fit is only illustrative, and no claim is made that $m = 0.9$ is an accurate description of the clumping distribution in the wind of WR 90. Modeling has shown that the winds of WC stars have rather extended acceleration zones to large radii (Hillier & Miller 1999; Gräfener & Hamann 2005), hence the underlying assumption of constant radial expansion in the region where the 10–20 micron emission forms may not be valid for WR 90. Still, this example application to *Spitzer* data shows that the FREC model can give qualitatively reasonable fits.

4 Summary

In this paper an elegant result originally derived by Hillier et al. (1983) has been expanded significantly to allow for

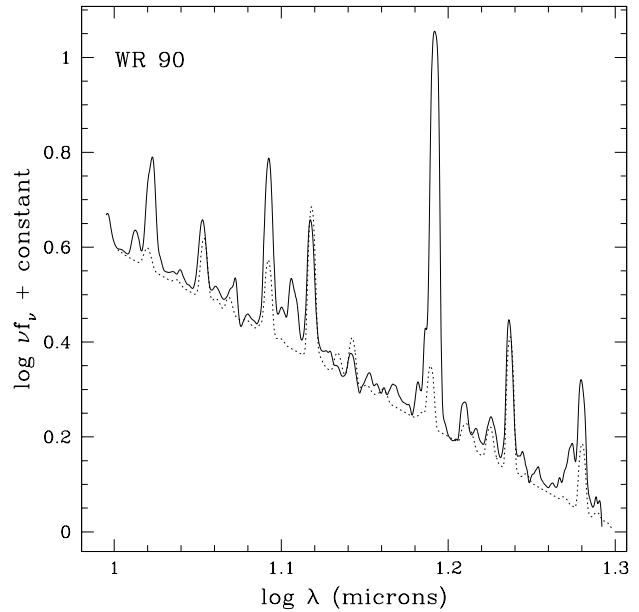


Fig. 5 Shown is *Spitzer* data for the WC star, WR 90 (solid), along with a model fit using the FREC model (dotted). This is a two-parameter fit: $m = 0.9$ is chosen to match the continuum slope, and the lines are governed by a single optical depth parameter assuming LTE for relative level populations. The spectrum has been gaussian convolved to the resolution of the IRS/SH instrument. The stronger lines of He II are approximately matched. Note the prominence of [Ne III] 15.55 microns, which is not part of the FREC and would need to be modeled separately (e.g., Smith & Houck 2005).

greater versatility. Although the assumptions remain restrictive (spherical symmetry, isothermal, and the constant radial expansion), the solution to the radiative transfer is analytic and allows for both line blends and a power-law dependence of the clumping with radius. The latter is especially significant since clumping is now understood to be an important consideration in deriving mass-loss rates from observations and since there are outstanding questions regarding the evolution of the clumping factor throughout stellar winds.

What is especially interesting about the new FREC models is a relation between line widths and line equivalent widths that has a dependence on the exponent m . Quantitatively the predicted relations may not be realized in data owing to the various assumptions built into making the FREC solution analytic; however, models based on the generalized line source functions from equation (16) may be new avenues of consideration for quick parameter exploration for those who use the more sophisticated radiative transfer techniques for spectral synthesis of stellar winds. Archival data from the *Infrared Space Observatory* or the *Spitzer* satellite may have adequate spec-

tral resolution for sources with fast winds to test against such relations and place limits on the variation of clumping with radius.

Although this paper focused on He II emission line spectra of WR winds for application, owing to the high densities of these winds, the solution may be applicable to other sources, like the hydrogen recombination line spectra of Luminous Blue Variable (LBV) stars, such as P Cygni (Lamers et al. 1996). The FREC solution may even have application data to suitable hypercompact or ultracompact H II regions. These sources show radio recombination lines and free-free continuum spectra plus evidence for density gradients (e.g., Keto, Qizhou, & Kurtz 2008).

Acknowledgements

I want to thank both the referee Wolf-Rainer Hamann and my good friend Joe Cassinelli for a number of helpful comments. I also gratefully acknowledge Greg Tracy for his efforts in reducing the *Spitzer* data of WR 90.

References

- Abbott D. C., Biegging J. H., Churchwell E. B., 1981, *ApJ*, 250, 645
- Abbott D. C., Biegging J. H., Churchwell E., Cassinelli, J. P., 1980, *ApJ*, 238, 196
- Auer L.-H., Mihalas, D., 1972, *ApJS*, 24, 193
- Berghöfer, T. W., Schmitt, J. H. M. M., Danner, R., Cassinelli, J. P., 1997, *A&A*, 322, 167
- Bouret J.-C., Lanz T., Hillier D. J., 2005, *A&A*, 438, 301
- Bouret J.-C., Lanz T., Hillier D. J., Heap, S. R., Hubeny, I., Lennon, D. J., et al., 2003, *ApJ*, 595, 1182
- Brown J. C., Cassinelli J. P., Li Q., Kholtygin A. F., Ignace R., 2004, *A&A*, 426, 323
- Carciofi, A., Bjorkman, J., 2006, *ApJ*, 639, 1081
- Cassinelli, J. P., 1979, *ARAA*, 17, 275
- Cassinelli, J. P., Hartmann, L., 1977, *ApJ*, 212, 488
- Cassinelli, J. P., Swank, J. H., 1983, *ApJ*, 271, 681
- Castor, J. I., 1970, *ApJ*, 160, 1187
- Castor, J. I., Abbott, D. C., Klein, R. I., 1975, *ApJ*, 195, 157
- Cox, A. N., 2000, *Allen's Astrophysical Quantities*, (New York: AIP Press)
- Dessart L., Owocki S. P., 2002, *A&A*, 383, 1113
- Dessart L., Owocki S. P., 2003, *A&A*, 406, L1
- Dessart L., Owocki S. P., 2005, *A&A*, 432, 281
- Evans, C. J., Crowther, P. A., Fullerton, A. W., Hillier, D. J., 2004, *ApJ*, 610, 1021
- Feldmeier A., Puls, J., Pauldrach, A. W. A., 1997, *ApJ*, 479, 231
- Friend, D. B., Abbott D. C., 1986, *ApJ*, 311, 701
- Fullerton A. W., Massa D. L., Prinja R. K., 2006, *ApJ*, 637, 1025
- Gräfener G., Koesterke L., Hamann W.-R., 2002, *A&A*, 387, 244
- Gräfener G., Hamann W.-R., 2005, *A&A*, 432, 633
- Gradshteyn, I. S., Ryzhik, I. M., 2000, *Table of Integrals, Series, and Products*, (Academic Press: San Diego)
- Groenewegen, M. A. T., Lamers, H. J. G. L. M., 1989, *A&AS*, 79, 359
- Hamann, W.-R., Feldmeier, A., Oskinova, L., 2008, *Clumping in Hot Star Winds*, (Univ. Verlag Potsdam: URN urn:nbn:de:kobv:517-opus-13981)
- Hummer, D. G., Rybicki, G. B., 1983, *ApJ*, 274, 380
- Hummer, D. G., Rybicki, G. B., 1985, *ApJ*, 293, 258
- Hillier D. I., 1991, *A&A*, 247, 455
- Hillier D. I., Jones, T. J., Hyland, A. R., 1983, *ApJ*, 271, 221
- Hillier D. I., Miller, D. L., 1998, *ApJ*, 496, 407
- Hillier D. I., Miller, D. L., 1999, *ApJ*, 519, 354
- Ignace R., Quigley M., Cassinelli J. P., 2003, *ApJ*, 596, 538
- Ignace R., Cassinelli J. P., Tracy, G., Churchwell, E., Lamers, H. J. G. L. M., 2007, *ApJ*, 669, 600
- Keto E., Zhang Q., Kurtz S., 2008, *ApJ*, 672, 423
- Kudritzki, R.-P., Puls, J., 2000, *ARAA*, 350, 970
- Lamers H. J. G. L. M., Cassinelli J. P. 1999, *Introduction to Stellar Winds*, New York, Cambridge University Press
- Lamers H. J. G. L. M., Cerruti-Sola M., Perinotto M., 1987, *ApJ*, 314, 726
- Lamers H. J. G. L. M., Najarro F., Kudritzki R. P., Morris P. W., Voors R. H. M., van Gent J. I., et al., 1996, *A&A*, 315, L229
- Leitherer, C., Chapman, J. M., Koribalski, B., 1995, *ApJ*, 450, 289
- Lucy, L. B., 1982, *ApJ*, 255, 278
- Lucy, L. B., Solomon, P. M., 1970, *ApJ*, 159, 879
- Maeder A., Meynet G., 2000, *A&A*, 38, 143
- Meynet G., Maeder A., 2003, *A&A*, 404, 975
- Morris P. W., Brownsberger, K. R., Conti, P. S., Massey, P., Vacca, W. D., 1993, *ApJ*, 412, 324
- Nugis T., Crowther P. A., Willis A. J., 1998, *A&A*, 333, 956
- Oskinova, L. M., Hamann, W.-R., Feldmeier, A., 2007, *A&A*, 476, 1331
- Oskinova, L. M., Ignace, R., Brown, J. C., Cassinelli, J. P., 2001, *A&A*, 373, 1009
- Owocki S. P., Castor, J. I., Rybicki, G. B., 1988, *ApJ*, 335, 914
- Pauldrach, A., Puls, J., Kudritzki, R. P., 1986, *A&A*, 164, 86
- Prinja, R. K., Barlow, M. J., Howarth, I. D., 1990, *ApJ*, 361, 607
- Runacres M. C., Owocki S. P., 2002, *A&A*, 381, 1015
- Runacres M. C., Owocki S. P., 2005, *A&A*, 429, 323
- Rybicki, G. B., Hummer, D. G., 1978, *ApJ*, 219, 654
- Smith, J.-D. T., Houck, J. R., 2005, *ApJ*, 622, 1044
- Woosely, S. E., Bloom, J. S., 2006, *ARAA*, 44, 507
- Wright, A. E., Barlow, M. J., 1975, *MNRAS*, 170, 41